PAPER

Topology of phase and polarisation singularities in focal regions

IOP Publishing Journal of Optics
J. Opt. **19** (2017) 105609 (8pp) https://doi.org/10.1088/2040-8986/aa895d

Topology of phase and polarisation singularities in focal regions

Petar Andrejic and John Lekner

School of Chemical and Physical Sciences, Victoria University of Wellington, PO Box 600, Wellington, New Zealand

Received 6 April 2017, revised 9 August 2017
Accepted for publication 31 August 2017
Published 22 September 2017

Abstract

The focal region of a beam contains circles of zeros of the beam wavefunction, on which surfaces of different phase meet. The existence of these zeros is topological in origin, and appears to be universal. Two examples of generalised Bessel beams are examined. One of these has zeros only in the focal plane. The other has focal plane zeros but also movement of the zeros away from the focal plane at certain values of a parameter which determines the tightness of the focus, as analysed by Berry in 1998. As tightness of focus increases these two families of beams coalesce into a common most-focused beam. The polarisation properties of both families and of their common limiting form are considered and correlated with the zeros (dislocations) of the beam wavefunctions. We find regions of circular polarisation in beams which are nominally linearly polarised, and rapid variation of the polarisation pattern as the tightness of focus passes through critical values.

Supplementary material for this article is available online

Keywords: phase singularities, focal region, optical vortices

(Some figures may appear in colour only in the online journal)

1. Introduction

The focal regions of beams (optical or acoustic) are the most interesting, experimentally and theoretically. A key property of the focal region is that it is where the wavefronts converge onto, and diverge from. In a monochromatic beam of angular frequency $\omega = ck$, the beam wavefunction carries an overall phase factor $e^{-i\omega t}$, and a local phase $P(\boldsymbol{r})$. The isophase surfaces $P(\boldsymbol{r}) =$ constant are the wavefronts (in an electromagnetic beam each component of $\boldsymbol{E}$ and $\boldsymbol{B}$ has, in general, its own set of wavefronts). The phase of a complex wavefunction is not defined at a zero of the wavefunction, where both the real and the imaginary parts are zero. This is where different isophase surfaces can meet. As time advances the surfaces on which $P(\boldsymbol{r}) - \omega t =$ constant rotate about the complex zeros of the beam wavefunction, and some authors call the zeros *optical vortices*. Nye and Berry [1] refer to these wavefunction zeros as *wave dislocations*. They are discussed in Nye's book [2], but the emphasis there is on natural focusing, as in the earlier studies of polarisations singularities by Berry and Dennis [3–5]. The emphasis in these papers is, like Nye's [2], mainly on properties 'in the wild' [4], random or disordered fields. The focal region, in contrast, is highly structured and symmetric.

Here we are interested in polarisation near the focus of a light beam. Karman *et al* [6, 7] have shown experimentally and theoretically that phase singularities in the focal region can be created and annihilated, and can move off the focal plane. An earlier numerical study by Carter [8] reported the same behaviour. Berry [9] and Nye [10] have given thorough discussions of this phenomenon; we shall follow Berry's classification here. Structured light itself is the subject of a recent roadmap [11], of which part 2 is a review of 'Vortices, natural and deliberate' by Berry and Dennis.

We shall discuss properties of exact ('non-paraxial') solutions of the Helmholtz equation $(\nabla^2 + k^2)\psi = 0$, which in cylindrical coordinates $(\rho,\ \phi,\ z)$ reads

$$(\partial_\rho^2 + \rho^{-1}\partial_\rho + \rho^{-2}\partial_\phi^2 + \partial_z^2)\psi = 0. \tag{1}$$

The Helmholtz equation is solved by $J_0(\kappa\rho)e^{im\phi}e^{iqz}$ provided that the transverse and longitudinal wavenumber components κ and q are constrained by $\kappa^2 + q^2 = k^2$. Superpositions of

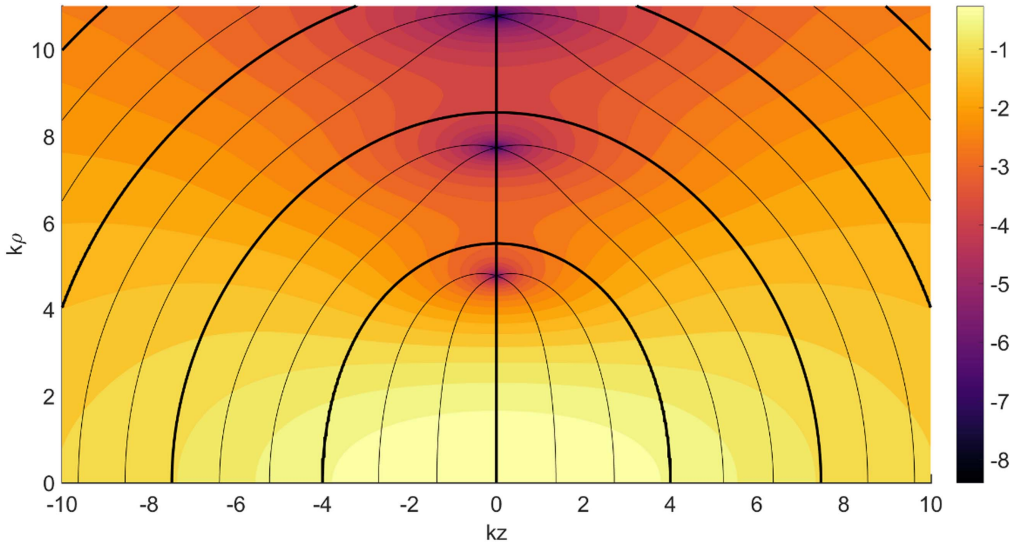

Figure 1. $\psi_b(\rho, z)$ in the focal region, plotted for $kb = 2$, for $k|z| \leqslant 10$, $k\rho \leqslant 10$. Shading indicates modulus of the wavefunction (logarithmic scale, lighter colour indicates larger modulus). The isophase surfaces are shown at intervals of $\pi/3$. The phase is chosen to be zero at the origin. The isophase contours, other than those that are multiples of π, meet on the zeros of $\psi_b(\rho, z)$, three of which are shown, at $k\rho \approx 4.77$, 7.73 and 10.77.

such solutions with a weight function $f(k, \kappa)$ give generalised Bessel beams [12],

$$\psi(\rho, \phi, z) = \mathrm{e}^{\mathrm{i}m\phi}\int_0^k \mathrm{d}\kappa f(k, \kappa) J_m(\kappa\rho)\mathrm{e}^{\mathrm{i}qz}, \quad \kappa^2 + q^2 = k^2. \tag{2}$$

We shall be considering beams with no azimuthal dependence, $m = 0$. The beam studied by Carter [8] and by Berry [9] is of the generalised Bessel beam form,

$$\psi_C(\rho, z) = \frac{b}{k}\left[1 - \mathrm{e}^{-\frac{kb}{2}}\right]^{-1}\int_0^k \mathrm{d}\kappa\ \kappa\ \mathrm{e}^{-\frac{b\kappa^2}{2k}+\mathrm{i}qz} J_0(\kappa\rho). \tag{3}$$

We have normalised the beam wavefunction to unity at the origin, the centre of the focal region. The (positive) length b and the wavenumber $k = \omega/c$ together form the dimensionless parameter kb which characterises the beam. The weight factor $\mathrm{e}^{-\frac{b\kappa^2}{2k}}$ is related to the Gaussian beam, an approximate (paraxial) solution of (1): the integral in (3) extended to the range $0 \leqslant \kappa < \infty$ reproduces, in the focal plane, the paraxial Gaussian fundamental mode, $\psi_G(\rho, z) = \frac{b}{b+\mathrm{i}z}\mathrm{e}^{\mathrm{i}kz - k\rho^2/2(b+\mathrm{i}z)}$ (see [13], appendix C). However, it is shown in [13] that an exact solution of the Helmholtz equation which agrees with ψ_G, either in the focal plane or on the beam axis, does not exist.

The wavefunction (3) shows the phenomena mentioned above, of phase singularities in the focal region being created and annihilated, and moving off the focal plane. In contrast, the wavefunction [12]

$$\psi_b(\rho, z) = \frac{b^2}{\mathrm{e}^{kb}(kb-1)+1}\int_0^k \mathrm{d}\kappa\ \kappa\ \mathrm{e}^{q(b+\mathrm{i}z)} J_0(\kappa\rho) \tag{4}$$

has all of its zeros in the focal plane. (Again, the prefactor ensures that the wavefunction is normalised to unity at the origin, $\psi_b(0, 0) = 1$.) As the dimensionless parameter kb tends to zero, both (3) and (4) tend to the proto-beam of [12],

$$\begin{aligned}\psi_0(\rho, z) &= \frac{2}{k^2}\int_0^k \mathrm{d}\kappa\ \kappa\ \mathrm{e}^{\mathrm{i}qz} J_0(\kappa\rho) \\ &= \frac{2}{k^2}\int_0^k \mathrm{d}q\ \ q\ \mathrm{e}^{\mathrm{i}qz} J_0(\kappa\rho).\end{aligned} \tag{5}$$

The proto-beam is the most tightly focused confluent limit of the two beam families (3) and (4). Only one length (k^{-1}) enters into its definition, and indeed the extent of its focal region, both longitudinally and transversely, is of order k^{-1} ([12], section 8). The proto-beam has all of its zeros in the focal plane, where $\psi_0(\rho, 0) = 2J_1(k\rho)/k\rho$.

In this paper we shall compare and contrast the two beam families (3) and (4), both characterised by the tightness of focus parameter kb. We begin in sections 2 and 3 with the isophase surfaces and loci of the wavefunction zeros as functions of kb. Sections 4 and 5 discuss the polarisation of the electric field in beams based on these two families and on their confluent tight-focus form.

2. Properties of the beam wavefunction $\psi_b(\rho, z)$

On the beam axis $\rho = 0$ the wavefunction (4) becomes

$$\begin{aligned}\psi_b(0, z) &= \frac{b^2}{\mathrm{e}^{kb}(kb-1)+1}\int_0^k \mathrm{d}q\ q\ \mathrm{e}^{q(b+\mathrm{i}z)} \\ &= \left(\frac{b}{b+\mathrm{i}z}\right)^2 \frac{\mathrm{e}^{k(b+\mathrm{i}z)}[k(b+\mathrm{i}z)-1]+1}{\mathrm{e}^{kb}(kb-1)+1}.\end{aligned} \tag{6}$$

$\psi_b(0, z)$ behaves asymptotically as a constant times $(kz)^{-1}\mathrm{e}^{\mathrm{i}kz}$. There are no wavefunction zeros on the beam axis.

Figure 1 shows the isophase surfaces of ψ_b. All of the zeros of ψ_b lie in the focal plane $z = 0$, and so the surfaces of negative phase from the $z < 0$ half-plane meet the surfaces of positive phase from the $z > 0$ half-plane on the focal plane,

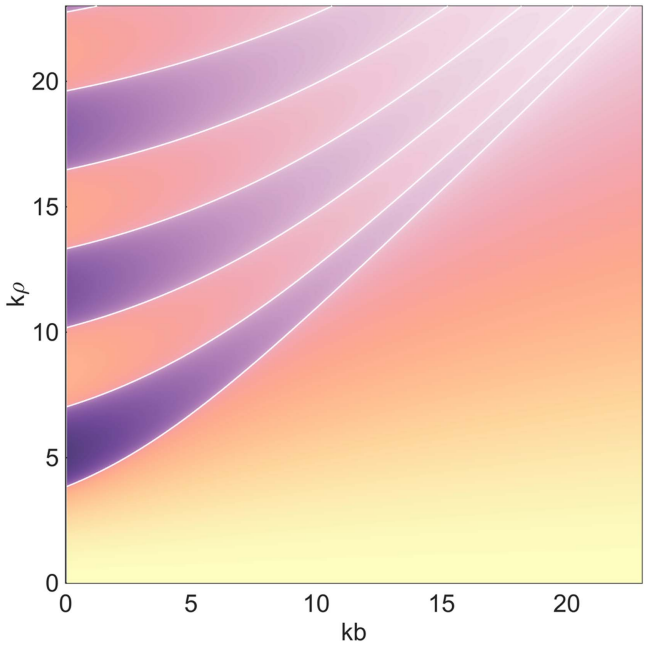

Figure 2. Zeros of $\psi_b(\rho, 0)$ as a function of kb (white curves). Also shown are the wavefunction focal plane values (negative: dark shading; zero: white; positive: light shading). As $kb \to 0$ the wavefunction zeros tend to those of the proto-beam. These are the zeros of $J_1(k\rho)/k\rho$, at $k\rho \approx 3.83,\ 7.02,\ 10.17,\ 13.32, \ldots$.

for all values of kb. The three-dimensional picture is obtained by rotating the figure about the beam (horizontal) axis.

Figure 2 shows how the focal plane zeros of ψ_b vary with the parameter $kb = \omega b/c$. (The length b determines the extent of the focal region: for large kb it gives the longitudinal extent, $\sqrt{2b/k}$ gives the beam waist in the focal plane, and $\sqrt{2/kb}$ is the divergence angle of the beam far from focus as shown in [13], appendix A.) We see from the figure that the zeros move outward from the beam axis as kb increases.

3. Properties of the Carter beam wavefunction

The Carter wavefunction shows topologically different behaviour, except at small kb.

On the beam axis $\rho = 0$ the Carter wavefunction (3) becomes

$$\psi_C(0, z) = \frac{b}{k}\left[e^{\frac{kb}{2}} - 1\right]^{-1}\int_0^k dqq\ e^{\frac{bq^2}{2k}+iqz}. \tag{7}$$

The integral may be evaluated in terms of error functions. It behaves asymptotically as a constant times $(kz)^{-1}e^{ikz}$. There are no wavefunction zeros on the beam axis.

Figure 3 shows the curves on which the real and imaginary parts of the wavefunction $\psi_C(\rho, z)$ are zero, in the kz, $k\rho$ plane. Where they meet gives the location of the complex zeros of ψ_C, which lie on circles centred on the beam axis.

In the six diagrams shown, we transition from all complex zeros on the focal plane (up to $kb = 4.919\,61$), to on-plane plus off-plane zeros ($kb = 5.152\,79$ to $5.254\,77$), beyond which the innermost focal region shown has off-plane zeros only.

Berry [9] has identified *three topological events* in ψ_C as the focal tightness parameter kb increases ($kb \to 0$ gives the tightest focus, the confluence of ψ_b and ψ_C into the proto-beam ψ_0). These are events that involve the phase dislocations, where $\psi = 0$, and phase saddles, where $\nabla P = 0$. The phase saddles or stagnation points can be seen clearly on figure 1: they occur between the zeros at circles where the integer π phases (thicker isophase curves) intersect the focal plane. The topological events in ψ_C are:

Event a, at $kb = 4.919\,61$. Lower saddle passes through upper zero.

Event b, at $kb = 5.152\,79$. Lower saddle collides with upper saddle.

Event c, at $kb = 5.254\,77$. Lowest two zeros coalesce.

The zeros in the focal plane $z = 0$ are zeros of the function

$$k^{-2}\int_0^k d\kappa\ \ \kappa\, e^{-\frac{b\kappa^2}{2k}} J_0(\kappa\rho) = \int_0^1 d\xi\ \ \xi\, e^{-(kb/2)\xi^2} J_0(k\rho\xi) = F(k\rho, kb). \tag{8}$$

The saddle points in the focal plane are at zeros of the function

$$k^{-3}\int_0^k d\kappa\ \ \kappa\sqrt{k^2-\kappa^2}\, e^{-\frac{b\kappa^2}{2k}} J_0(\kappa\rho) = \int_0^1 d\xi\ \ \xi\sqrt{1-\xi^2} \times e^{-(kb/2)\xi^2} J_0(k\rho\xi) = G(k\rho, kb). \tag{9}$$

Event a corresponds to $F(k\rho, kb) = 0 = G(k\rho, kb)$. The first three numerical values of $(k\rho, kb) = (\alpha_n, \beta_n)$ at which this happens are (to five digit accuracy)

$$\begin{aligned} \alpha_1 &= 7.4395 \quad \alpha_2 = 13.843 \quad \alpha_3 = 20.183 \\ \beta_1 &= 4.9196 \quad \beta_2 = 10.634 \quad \beta_3 = 16.549. \end{aligned} \tag{10}$$

Event b corresponds to $G(k\rho, kb) = 0 = \partial_\rho G(k\rho, kb)$. The first three numerical values of $(k\rho, kb) = (\alpha_n, \beta_n)$ at which this happens are

$$\begin{aligned} \alpha_1 &= 8.0277 \quad \alpha_2 = 14.401 \quad \alpha_3 = 20.721 \\ \beta_1 &= 5.1528 \quad \beta_2 = 10.856 \quad \beta_3 = 16.760. \end{aligned} \tag{11}$$

Event c corresponds to $F(k\rho, kb) = 0 = \partial_\rho F(k\rho, kb)$. The first three numerical values of $(k\rho, kb) = (\alpha_n, \beta_n)$ at which this happens are

$$\begin{aligned} \alpha_1 &= 7.0156 \quad \alpha_2 = 13.324 \quad \alpha_3 = 19.616 \\ \beta_1 &= 5.2548 \quad \beta_2 = 11.206 \quad \beta_3 = 17.287. \end{aligned} \tag{12}$$

The numerical values for α_1, β_1 agree in each case with those listed in the penultimate row of table 1 of Berry [9], with the parameter L corresponding to our $\sqrt{kb}$.

Figure 4 shows the zeros of the Carter wavefunction in the focal plane. As kb increases from zero the null curves initially move further away from the beam axis $\rho = 0$, but not as rapidly as for ψ_b in figure 2. However, they eventually

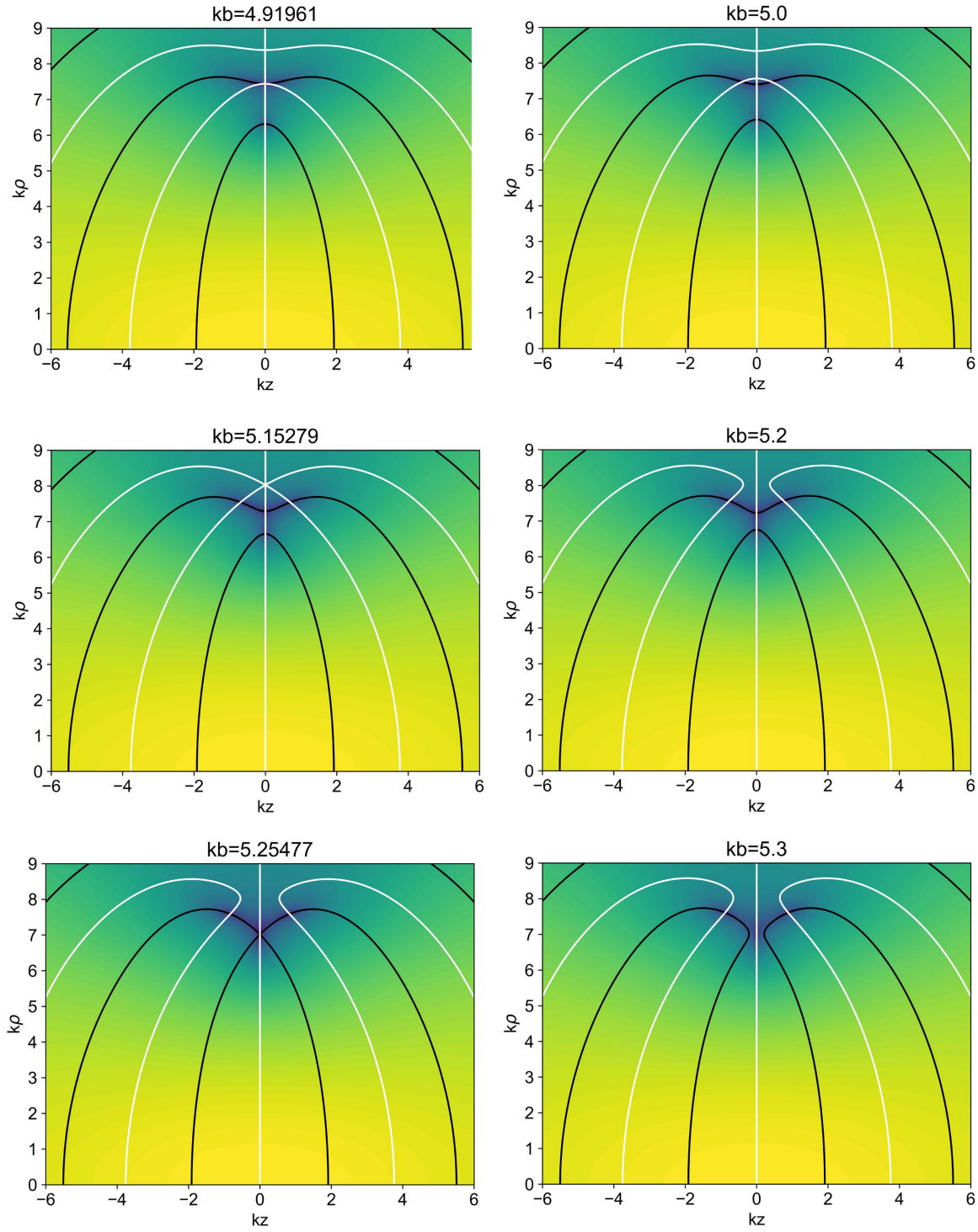

Figure 3. Surfaces of $\mathrm{Re}(\psi_C) = 0$ (black) and $\mathrm{Im}(\psi_C) = 0$ (white) in the focal region, for six values of kb. Included are three transition values $kb = 4.919\,61,\ 5.152\,79,\ 5.254\,77$, discussed in the text. The three-dimensional picture is obtained by rotating the figures about the beam (horizontal) axis. The shading is in proportion to the logarithm of $|\psi_C|$.

curve towards each other, and meet in pairs. The topological events identified by Berry are shown as points on this graph. It is interesting that for $kb < 4.919\,61$ all the zeros lie on the focal plane; it is only as we *loosen* the focus that the off-plane zeros appear.

4. Polarisation properties of TM, TE and 'LP' beams

We shall work with complex vector fields $\boldsymbol{A}(\boldsymbol{r})$, $\boldsymbol{B}(\boldsymbol{r})$, $\boldsymbol{E}(\boldsymbol{r})$; the real physical fields are obtained by taking, for example, the real part of $\boldsymbol{E}(\boldsymbol{r})\mathrm{e}^{-\mathrm{i}\omega t}$, which is $\boldsymbol{E_r}(\boldsymbol{r})\cos\omega t + \boldsymbol{E_i}(\boldsymbol{r})\sin\omega t$. A

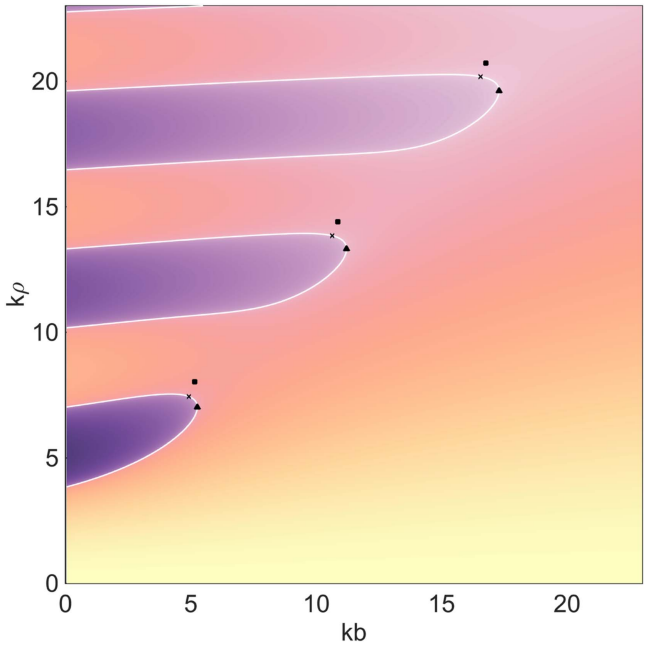

Figure 4. Variation with kb of the focal plane zeros of the Carter wavefunction (3) (white curves). Also shown are the wavefunction focal plane values (shading, as in figure 2). At $kb = 0$ the wavefunction zeros are again those of $J_1(k\rho)/k\rho$, as in figure 2. The transition points *a, b, c* discussed in the text are indicated by crosses, squares and triangles, respectively.

measure of the *degree of linear polarisation* of the electric field is given by [14]

$$\Lambda(\boldsymbol{r}) = \frac{[(E_r^2 - E_i^2)^2 + 4(\boldsymbol{E}_r \cdot \boldsymbol{E}_i)^2]^{\frac{1}{2}}}{E_r^2 + E_i^2} = \frac{|\boldsymbol{E}^2(\boldsymbol{r})|}{|\boldsymbol{E}(\boldsymbol{r})|^2}. \tag{13}$$

$\Lambda(\boldsymbol{r})$ is unity when the real and imaginary parts of $\boldsymbol{E}(\boldsymbol{r}) = \boldsymbol{E}_r(\boldsymbol{r}) + \mathrm{i}\boldsymbol{E}_i(\boldsymbol{r})$ are collinear (the linear polarisation condition), and zero when the circular polarisation conditions $\{\boldsymbol{E}_r \cdot \boldsymbol{E}_i = 0,\ E_r^2 = E_i^2\}$ are met. The complex electric field $\boldsymbol{E}(\boldsymbol{r})$ is orthogonal to itself on these C lines [11]: $\boldsymbol{E}(\boldsymbol{r}).\boldsymbol{E}(\boldsymbol{r}) = 0$. Explicit expressions for $\Lambda(\boldsymbol{r})$ in terms of the derivatives of ψ with respect to ρ and z when ψ is independent of the azimuthal angle ϕ are given in [14]. The function $\Lambda(\boldsymbol{r})$ is related to the Stokes parameters ([15], sections 1.4.2 and 10.8.3) by $\Lambda = \sqrt{1 - S_3^2/S_0^2}$, and to the Hurwitz [16] polarisation parameter S by $S^2 + \Lambda^2 = 1$.

The simplest example of pure linear polarisation is the TM (transverse magnetic) beam, for which the vector potential is given by $\boldsymbol{A} = A_0[0, 0, \psi]$. (See for example [14]; square brackets denote Cartesian coordinates.) For this beam the magnetic field $\boldsymbol{B}$ is everywhere transverse to the propagation direction, here along the z axis:

$$\boldsymbol{B} = \nabla \times \boldsymbol{A} = A_0[\partial_y, -\partial_x, 0]\psi. \tag{14}$$

When ψ is independent of the azimuthal angle ϕ the complex magnetic field is

$$\boldsymbol{B}(\boldsymbol{r}) = A_0[\sin\phi\partial_\rho, -\cos\phi\partial_\rho, 0]\psi. \tag{15}$$

If we take A_0 real, and write the complex wavefunction $\psi(\rho, z)$ as $\psi_r + \mathrm{i}\psi_i$, the real and imaginary parts of $\boldsymbol{B}(\boldsymbol{r})$ are both proportional to $[\sin\phi, -\cos\phi, 0]$, and are thus collinear. The magnetic field is therefore everywhere linearly polarised. The electric field is elliptically polarised, in general.

The dual of the TM beam under the transformation $\boldsymbol{E} \to \boldsymbol{B}, \boldsymbol{B} \to -\boldsymbol{E}$ (one of a set of duality transformations that leave the free space Maxwell equations unchanged) is the TE beam, transverse and linearly polarised in its electric field. The electric field lines are circles concentric with the beam axis (see figure 1 of [14], for example). However, both the TM and the TE beams disappear in the plane-wave limit: as $\psi \to \mathrm{e}^{\mathrm{i}kz}$ the electric and magnetic fields in both the TM and the TE beams tend to zero. Also, the fields are always zero on the beam axis; on both counts the exactly linearly polarised TE beam is not as interesting experimentally as the 'linearly polarised' beam about to be considered.

A beam which does have a plane-wave limit is the linearly polarised 'LP' beam, with vector potential $\boldsymbol{A} = A_0[\psi, 0, 0]$. The reason for the quotes around 'LP' is that the electric polarisation is everywhere linear only in the plane wave limit. As we shall see, the deviation from linear polarisation in finite beams is substantial, especially in the focal region. The magnetic and electric fields are

$$\begin{aligned}\boldsymbol{B} &= \nabla \times \boldsymbol{A} = A_0[0, \partial_z, -\partial_y]\psi,\\ \boldsymbol{E} &= \frac{\mathrm{i}}{k}\nabla(\nabla \cdot \boldsymbol{A}) + \mathrm{i}k\boldsymbol{A} = \frac{\mathrm{i}A_0}{k}[\partial_x^2 + k^2, \partial_x\partial_y, \partial_x\partial_z]\psi.\end{aligned} \tag{16}$$

In the plane wave limit $\psi \to \mathrm{e}^{\mathrm{i}kz}$, $\boldsymbol{B} \to \mathrm{i}kA_0[0, 1, 0]\mathrm{e}^{\mathrm{i}kz}$, $\boldsymbol{E} \to \mathrm{i}kA_0[1, 0, 0]\mathrm{e}^{\mathrm{i}kz}$, which is the textbook linearly polarised plane wave with $\boldsymbol{E}$ and $\boldsymbol{B}$ transverse and mutually perpendicular. We again consider beams defined by wavefunctions ψ independent of the azimuthal angle ϕ with the intention to use the wavefunctions ψ_0, ψ_b and ψ_C as examples. Then

$$\boldsymbol{B} = \mathrm{i}kA_0[0, \partial_z, -\sin\phi\partial_\rho]\psi, \tag{17}$$

$$\begin{aligned}\boldsymbol{E} = \frac{\mathrm{i}A_0}{k}[&\cos^2\phi\partial_\rho^2 + \sin^2\phi\rho^{-1}\partial_\rho + k^2,\\ &\sin\phi\cos\phi[\partial_\rho^2 - \rho^{-1}\partial_\rho],\ \cos\phi\partial_\rho\partial_z]\psi.\end{aligned} \tag{18}$$

Neither $\boldsymbol{E}$ nor $\boldsymbol{B}$ have real and imaginary parts collinear in general, but in the focal plane if $\partial_\rho\partial_z\psi = 0$ the longitudinal component of $\boldsymbol{E}$ will be zero and the transverse components will both be real, so only $\boldsymbol{E}_r$ is non-zero. Hence there can be circles of exact linear polarisation in the focal plane. The electric field is also linearly polarised (along the x direction) in the $x = 0$ plane ($\cos\phi = 0$), as can be seen from (18). By symmetry the beam wavefunction is plane wave like (and thus has linear polarisation) at the centre of the focal plane.

5. Polarisation properties of 'LP' beams based on ψ_0, ψ_b and ψ_C

We shall look at the consequences of the phase singularities for the polarisation properties of an electromagnetic 'LP' beam built up from the scalar beam wavefunctions (3), (4) and (5). From (18) the electric polarisation depends on the wavefunction and on its derivatives $\partial_\rho\psi$, $\partial_\rho^2\psi$, $\partial_\rho\partial_z\psi$. For the proto-beam ψ_0 all these derivatives are known analytically

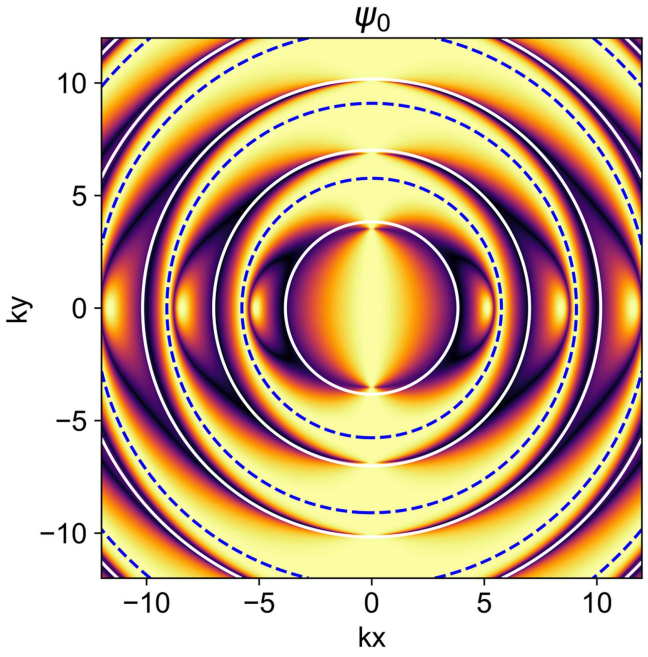

Figure 5. Degree of electric field linear polarisation Λ for a 'linearly polarised' ψ_0 beam, in the focal plane. Light shading denotes linear and dark shading circular polarisations. The white circles are the zeros of ψ_0, namely those of $J_1(k\rho)/k\rho$. The dashed circles are loci of perfect linear polarisation, $\Lambda = 1$, as discussed in the text. On the horizontal axis ($y = 0$) there are points of perfect circular polarisation, also discussed in the text.

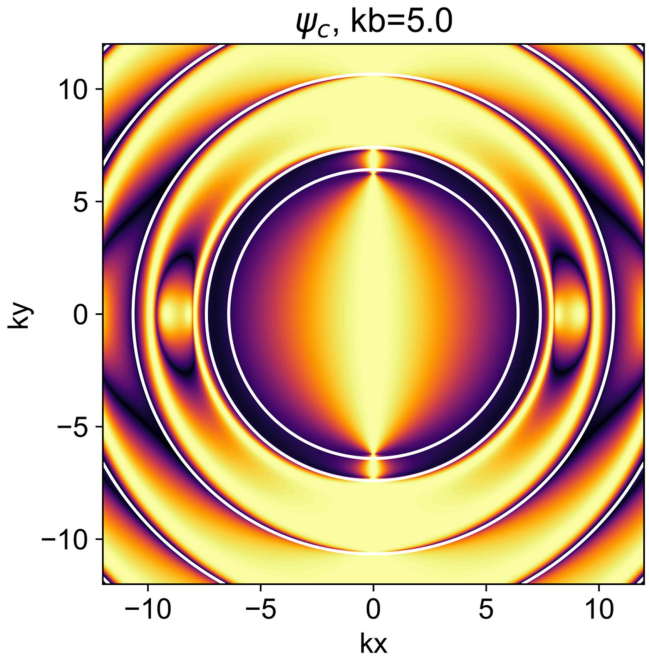

Figure 6. The measure Λ of linear polarisation of the electric field of an 'LP' beam based on ψ_C, shown in the focal plane for $kb = 5$ Light colour denotes linear and dark colour circular polarisations. There are circles of perfect linear polarisation when $\partial_\rho\partial_z\psi = 0$, at $k\rho \approx 7.9,\ 9.9\ldots$. Note the correlation of the deviation from linear polarisation with the circles of zero ψ (white), especially between the innermost pair of zeros which occur at $k\rho \approx 6.4$ and 7.4 when $kb = 5$. An animation for variable kb is available in the supplementary material online (stacks.iop.org/JOPT/19/105609/mmedia).

in the focal plane (equations (5.16)–(5.20) of [12]). Figure 5 shows the degree of linear polarisation for an 'LP' beam derived from ψ_0. We see that there is perfect linear polarisation at the centre of the focal plane, on the $x = 0$ plane ($\cos\phi = 0$, so only E_x is non-zero, from (18)), and also on circles where the spherical Bessel function $j_2(k\rho)$ is zero, since $\partial_\rho\partial_z\psi_0$ at $z = 0$ is proportional to i times $j_2(k\rho)$. The other derivatives entering into the expression (17) for the electric field are real in the focal plane, so when $j_2(k\rho) = 0$ the electric vector is real, and $\Lambda = 1$.

More surprising is the fact that perfect *circular* polarisation exists, not far from the centre of the focal region. On the x axis, when $\sin\phi = 0,\ \cos\phi = \pm 1$, the electric field of (17) is proportional to $[\partial_\rho^2 + k^2,\ 0,\ \pm\partial_\rho\partial_z]\psi$. For the proto-beam we have from [12], equations (51.5), (5.17) and (5.19) that

$$(\partial_\rho^2 + k^2)\psi_0 = 6(k\rho)^{-3}[2J_1(k\rho) - k\rho J_0(k\rho)], \qquad (19)$$

$$\partial_\rho\partial_z\psi_0 = -2\mathrm{i}(k\rho)^{-1}j_2(k\rho). \qquad (20)$$

Hence when the expressions (19) and (20) are equal in magnitude the electric field will be proportional to $[1,\ 0,\ \pm\mathrm{i}]$, corresponding to perfect circular polarisation in the xz plane. The C lines intersect the focal plane at $k|x| \approx 3.98,\ 5.44,\ 6.94,\ 8.79,\ldots$. The points nearest to the focal centre, at $kx \approx \pm 3.98$, $y = 0$, $z = 0$, have electric field magnitude equal to 18.6% of the field at the centre, a significant fraction.

Figure 6 shows how the polarisation of the 'LP' Carter beam varies with position, when the tightness of focus parameter $kb = 5$. Note that there is a very strong deviation from linear polarisation between the inner two zeros of ψ_C, which are about to coalesce (event c, at $kb \approx 5.255$, as discussed in section 3). The beam is linearly polarised at the centre of the focal region, by design, and there are also circles of linear polarisation in the focal plane at distances from the beam axis where $\partial_\rho\partial_z\psi = 0$. An animation of the changes that occur as kb increases through the transition values discussed in section 3 is available online. Figure 7 shows the polarization of a 'linearly polarized' beam based on the wavefunction ψ_b defined in (4).

6. Discussion

We have compared two families of beams ψ_C and ψ_b, and of their common tight focusing limit ψ_0. The beam wavefunction ψ_C given in (3) was proposed in 1973 by Carter [8] and the topology of its phase singularities was analysed by Berry [9]. This cylindrically symmetric wavefunction is parametrised by kb, where $k = \omega/c$ is the wavenumber, and b is a length. The Carter wavefunction isophase surfaces meet on the wavefunction zeros which, for values of the dimensionless parameter kb smaller than the critical value 4.91961, all lie on circles in the focal plane. However, at larger kb values the interplay of the evolution of the surfaces on which

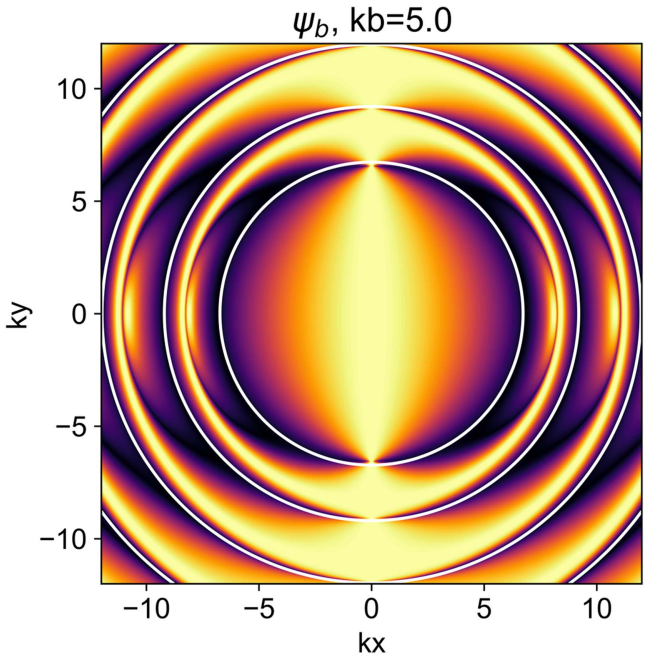

Figure 7. The measure Λ of linear polarisation of the electric field of an 'LP' beam based on ψ_b, shown in the focal plane for $kb = 5$. Light colour denotes linear and dark colour circular polarisations. There are circles of perfect linear polarisation when $\partial_\rho \partial_z \psi = 0$, at $k\rho \approx 8.4,\ 11.2 \ldots$. Note the correlation of the deviation from linear polarisation with the circles of zero ψ (white), the first three of which occur at $k\rho \approx 6.7,\ 9.2$ and 12.0 when $kb = 5$.

$\mathrm{Re}(\psi_C) = 0$ and $\mathrm{Im}(\psi_C) = 0$ and of their intersections (on the complex zeros of ψ_C) produces zeros which lie off the focal plane. This behaviour was shown numerically by Carter, and classified by Berry. The wavefunction ψ_b defined in (4) forms a family also characterised by the parameter kb which determines the tightness of focus.

The wavefunctions ψ_C and ψ_b coalesce into the proto-beam ψ_0 as $kb \to 0$, but become topologically different at intermediate and large values of the parameter kb. It is interesting that the *loosening of the focus* leads to the differentiation. To see the reason for the differences we shall compare the weight functions of ψ_C and ψ_b. In terms of the dimensionless variables $\alpha = k\rho,\ \beta = kb,\ \eta = q/k,\ \zeta = kz$ we can write the beam wavefunctions (normalised to unity at the origin) as

$$\psi_C = \frac{\beta \mathrm{e}^{\,\beta/2}}{\mathrm{e}^{\,\beta} - 1} \int_0^1 \mathrm{d}\eta\ \eta\ \mathrm{e}^{\left(\frac{\beta}{2}\right)\eta^2 + \mathrm{i}\zeta\eta} J_0(\alpha\sqrt{1-\eta^2}) = \int_0^1 \mathrm{d}\eta\ W_C(\beta,\eta)\ \mathrm{e}^{\mathrm{i}\zeta\eta} J_0(\alpha\sqrt{1-\eta^2}), \tag{21}$$

$$\psi_b = \frac{\beta^2}{\mathrm{e}^{\beta(\beta-1)+1}} \int_1^0 d\eta\ \ \eta \mathrm{e}^{(\beta+\mathrm{i}\zeta)\eta} J_0(\alpha\sqrt{1-\eta^2}) = \int_1^0 \mathrm{d}\eta\ W_b(\beta,\eta)\ \mathrm{e}^{\mathrm{i}\zeta\eta} J_0(\alpha\sqrt{1-\eta^2}). \tag{22}$$

The weight functions of these generalised Bessel beams are

$$W_C(\beta,\eta) = \frac{\beta \mathrm{e}^{\beta/2}}{\mathrm{e}^{\beta} - 1} \eta \mathrm{e}^{\left(\frac{\beta}{2}\right)\eta^2}, \qquad W_b(\beta,\eta) = \frac{\beta^2}{\mathrm{e}^{\beta(\beta-1)+1}} \eta \mathrm{e}^{\beta\eta}. \tag{23}$$

The weight function W_C is always larger at small η (small longitudinal wavevector component q), exponentially so at large $\beta = kb$. W_b is always larger as $\eta \to 1$ ($q \to k$). The weight functions are equal at

$$\eta_c = \left(\frac{q}{k}\right)_c = 1 - \sqrt{1 + \frac{2}{\beta} \ln\left[\frac{\beta(\mathrm{e}^{\beta/2} - 1)}{\mathrm{e}^{\beta}(\beta - 1)}\right]}. \tag{24}$$

This cross over value of q/k is always greater than $1 - 6^{-\left(\frac{1}{2}\right)} \approx 0.59$ (its limiting value at $\beta \to 0$), and tends to unity for large β as $1 - \sqrt{2}\ \beta^{-1}$. Thus the Carter beam emphasises the transverse component κ of the wavevector, while ψ_b emphasises the longitudinal wavevector component q. The function ψ_b is the more 'paraxial' beam wavefunction at large kb, as is seen in the comparison of exact and paraxial beam wavefunctions in [13].

Section 5 explored the polarisation properties of 'LP' beams based on these three wavefunctions. Of importance in experiments where the polarisation of an electromagnetic beam is involved, is the very strong effect that the wavefunction zeros (on and off the focal plane) have on the polarisation of the light beam. We showed examples of beams linearly polarised in the plane wave limit, yet with regions of circular polarisation surrounding the central focal region, located near the wavefunction zeros. In the most tightly focused case, the perfect circular polarisation points nearest to the focal centre have electric field magnitude equal to a significant fraction of the field at the (linearly polarised) centre of the beam.

Berry [17] considered the connection between optical vortices and angular momentum, and between circular polarisation singularities and angular momentum, concluding that there is usually no connection. Here we saw that the zeros of the beam wavefunction are strongly correlated with polarisation anomalies.

Acknowledgments

This paper has benefitted from Reviewer comments and suggestions.

ORCID iDs

John Lekner https://orcid.org/0000-0003-4675-9242

References

[1] Nye J F and Berry M V 1974 Dislocations in wave trains *Proc. R. Soc.* A **336** 165–90
[2] Nye J F 1999 *Natural Focusing and the Fine Structure of Light* (Bristol: Institute of Physics Publishing)
[3] Berry M V and Dennis M R 2001 Polarization singularities in isotropic random vector waves *Proc. R. Soc.* A **457** 141–55
[4] Dennis M R 2002 Polarization singularities in paraxial vector fields: morphology and statistics *Opt. Commun.* **213** 201–21

[5] Berry M V 2004 Index formulae for singular lines of polarization *J. Opt. A: Pure Appl. Opt.* **6** 675–8
[6] Karman G P, Beijersbergen M W, van Duijl A and Woerdman J P 1997 Creation and annihilation of phase singularities in a focal field *Opt. Lett.* **22** 1503–5
[7] Karman G P, Beijersbergen M W, van Duijl A, Bouwmeester D and Woerdman J P 1998 Airy pattern reorganization and subwavelength structure in a focus *J. Opt. Soc. Am.* A **15** 884–99
[8] Carter W H 1973 Anomalies in the field of a Gaussian beam near focus *Opt. Commun.* **64** 491–5
[9] Berry M V 1998 Wave dislocation reactions in non-paraxial Gaussian beams *J. Mod. Opt.* **45** 1845–58
[10] Nye J F 1998 Unfolding of higher-order wave dislocations *J. Opt. Soc. Am.* **15** 1132–8
[11] Rubinstein-Dunlop H *et al* 2017 Roadmap on structured light *J. Opt.* **19** 013001
[12] Lekner J 2016 Tight focusing of light beams: a set of exact solutions *Proc. R. Soc.* A **472** 20160538
[13] Lekner J and Andrejic P 2017 Nonexistence of exact solutions agreeing with the Gaussian beam on the beam axis or in the focal plane *Opt. Commun.* **407** 22–6
[14] Lekner J 2003 Polarization of tightly focused laser beams *J. Opt. A: Pure Appl. Opt.* **5** 6–14
[15] Born M and Wolf E 1999 *Principles of Optics* 7th edn (Cambridge: Cambridge University Press)
[16] Hurwitz H 1945 The statistical properties of unpolarised light *J. Opt. Soc. Am.* **35** 525–31
[17] Berry M V 2009 Optical currents *J. Opt. A: Pure Appl. Opt.* **11** 094001